

Article

Modelling and Design Optimization of a Novel Compliant XY Positioner for Vibration-Assisted CNC Milling

Minh Phung Dang ^{1,*} , Chi Thien Tran ¹, Hieu Giang Le ¹, Vo Quoc Anh Tran ¹ and Hong Van Tran ²

¹ Faculty of Mechanical Engineering, Ho Chi Minh City University of Technology and Education, Ho Chi Minh City 700000, Vietnam

² Faculty of Automation Technology, Thu Duc College of Technology, Ho Chi Minh City 700000, Vietnam

* Correspondence: phungdm@hcmute.edu.vn

Abstract: Vibration-assisted machining, known as hybrid processing technology, offers several benefits over conventional machining methods. However, developing mechanical structure designs to generate a non-resonant frequency source remains challenging. The objective of this study is to propose a novel design for an XY flexure positioner by combining the pseudo-rigid-body model with the Lagrange technique, finite element analysis and Crayfish optimization algorithm. Firstly, the mechanism was designed by combining a hybrid amplifier and parallel driving mechanism integrated with right circular hinges to increase the natural frequency and precision for potential application to VAM CNC milling. Then, the analytical model was established by the pseudo-rigid-body and Lagrange method. Next, the theoretical result was verified by finite element analysis. The first natural frequency results of theory and FEM methods were found at 990.74 Hz and 1058.5 Hz, respectively. The error between the two methods was 6.4%, demonstrating a reliable modeling approach. Based on the analytical equations, the Crayfish optimization algorithm was utilized for optimizing the main design variables of the mechanism. Next, the prototype was fabricated. The results showed that the experimental and simulated frequencies were 1127.62 Hz and 1216.6 Hz, with an error between the two methods of 7.31%. Finally, the workpiece was installed on the prototype and a real vibration-assisted CNC milling process was carried out in the frequency range [700 Hz, 1000 Hz]. The best surface roughness of the specimen was achieved at a frequency of 900 Hz with a Ra of 0.287 μm . This demonstrates that the proposed XY mechanism is an effective structure for generating a non-resonant frequency source for vibration-assisted machining.

Keywords: hybrid machining; vibration-assisted CNC milling; compliant XY positioner; crayfish optimization algorithm; surface roughness



Citation: Dang, M.P.; Tran, C.T.; Le, H.G.; Tran, V.Q.A.; Tran, H.V.

Modelling and Design Optimization of a Novel Compliant XY Positioner for Vibration-Assisted CNC Milling. *Machines* **2024**, *12*, 534. <https://doi.org/10.3390/machines12080534>

Academic Editors: Bingxiao Ding, Jinqing Zhan and Nguyen Vu Linh

Received: 7 July 2024

Revised: 31 July 2024

Accepted: 1 August 2024

Published: 6 August 2024



Copyright: © 2024 by the authors. Licensee MDPI, Basel, Switzerland. This article is an open access article distributed under the terms and conditions of the Creative Commons Attribution (CC BY) license (<https://creativecommons.org/licenses/by/4.0/>).

1. Introduction

Hybrid machining is an advanced technology that integrates one or more conventional machining processes with new machining processes. Hybrid machining includes vibration-assisted machining (VAM), electrochemical discharge, laser, abrasive-water jet, and so on [1]. Among these advanced technologies, VAM is a non-resonant machining technique that has been developed for integration in CNC machines, aiding in areas such as vibration-assisted turning [2,3], vibration-assisted drilling [4,5], vibration-assisted milling [6–9], and EDM [10,11]. The VAM often operates at a non-resonant frequency mode of less than 10 kHz resonant frequency, while ultrasonic machining works at a resonant frequency mode more significant than 20 kHz. Controlling the frequency of the system during machining at the resonant frequency mode is not easy, and this system is relatively costly. In contrast, the VAM with non-resonant modes offers more benefits because the frequency control becomes easier [12]. Nowadays, the VAM has been applied to enhance the machining abilities of traditional CNC machines, including material removal rate, smooth surface quality, reduced surface roughness, decreased cutting forces, less tool wear, extended tool

life, improved chip removal, and reduced burr formation. The VAM is a particularly more effective machining technology in regard to processing hard materials [13].

The non-resonant models are able to adjust the frequency of a vibration source. The vibration source often comes from mechanical mechanisms or structures. Traditional rigid-link mechanisms can generate a non-resonant frequency model for VAM, but they exist in clearance and backlash that cause machining errors. In addition, traditional mechanisms also affect the environment due to the need for lubricants to reduce friction. These types are also very costly because of complex assembly. In contrast, compliant mechanisms can initialize a non-resonant frequency model by generating micro-scale motions and flexibility through elastic hinges without kinematic joints. Compliant mechanisms offer numerous benefits, such as zero lubricant, monolithic structure, high precision, smooth motion, and reduced assemble systems [14–18]. In addition, to generate a smooth motion for VAM, compliant mechanisms are integrated with piezoelectric actuators (PZTs) to generate a force on the mechanism, which is then transferred to a non-resonant VAM system. In the last decade, researchers have proposed many different designs for VAM devices.

For instance, in the fast tool servo, a two-degree of freedom (DOF) compliant mechanism was offered [19]. In VAM polishing, 2-3 DOF compliant mechanisms were designed [20–22]. Particularly, Gu et al. [20] proposed an XY stage that achieved a resonant frequency of 411.23 Hz. In this study, a four-lever amplification mechanism was integrated into a compliant XY stage for vibration-assisted polishing. Regarding VAM milling, 2 DOF compliant mechanisms were suggested [9,23,24]. More specifically, Pham et al. [23] proposed an XY stage which gained a natural frequency of 689 Hz. They integrated a single-lever displacement amplifier and hollow flexure hinges for vibration-assisted milling for AL6061 material. However, this study found it difficult to achieve a small parasitic motion error as well as a parallel motion with the feed directions due to the asymmetrical structure characteristic of a single-lever displacement amplifier.

Although the studies mentioned above in the literature have been proposed for VAM, the structures of compliant mechanisms still have some limitations, such as low stiffness, small non-resonant frequency, small working stroke, and large parasitic motion errors. Unlike the previous study, the authors of this paper are motivated to develop a new compliant positioner XY to generate a non-resonant frequency model for VAM CNC milling. The new aspects of the present study are summarized as follows.

- A symmetrical eight-lever displacement amplification mechanism combined with right circular joints has been developed to integrate into the proposed mechanism. Compared with other flexure hinges [25–28], the right circular hinges were proposed to integrate into the stage because of their highest rotation accuracy to achieve high position precision and reduce parasitic motion error. This design aims to minimize parasitic motion and enhance the stiffness as well as the natural frequency of the mechanism for VAM CNC milling.
- In order to improve the output response of the mechanism utilized in the vibration-assisted CNC milling process, a hybrid framework strategy is proposed by combining the pseudo-rigid-body model with the Lagrange technique, finite element analysis, and Crayfish optimization algorithm.

This paper aims to present a novel design of the XY compliant mechanism for applying in VAM CNC milling. The proposed XY mechanism is built based on the hybrid amplification mechanism and the parallel driving mechanism with the right circular hinges. The static and dynamic equations are theoretically formulated, and the theory's accuracy is assessed by finite element analysis. The output response of the mechanism is optimized by the Crayfish optimizer. The prototype is manufactured. Finally, the VAM CNC milling experiments are performed to evaluate the effectiveness of the proposed XY mechanism.

2. Mechanical Design

The objective of this study is to develop an innovative vibration-assisted compliant positioner that can be used in the CNC milling process to improve the surface roughness

of manufactured parts. Moreover, the utilization of the non-resonant technique is implemented to generate vibrations within the workpiece through the utilization of a stage. The structure is specifically built by using a symmetrical four-lever amplification mechanism (LAM) integrated with right circular hinges according to the highest rotation center accuracy in order to reduce parasitic motion error, as depicted in Figure 1. Specifically, the proposed hybrid displacement amplifier has three floors, including LAM 1 of the first floor, LAM 2 and LAM 3 of the second floor and LAM 4 of the third floor, as illustrated in Figure 1.

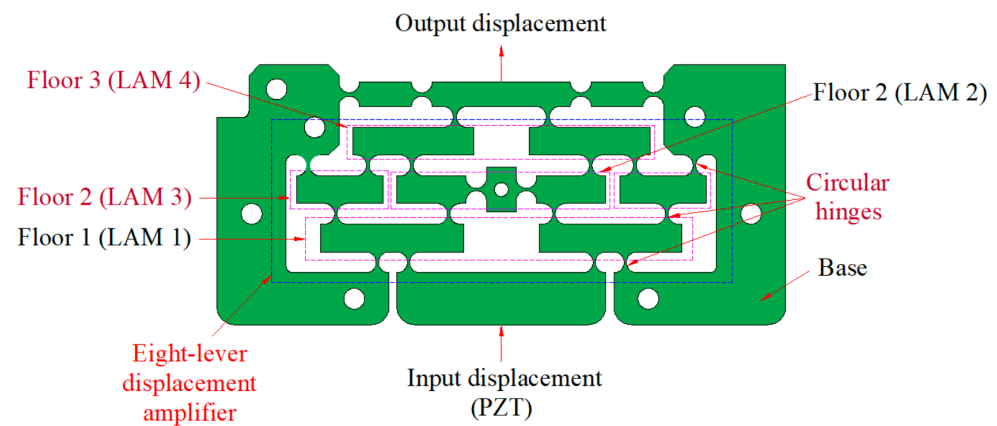


Figure 1. Proposed eight-lever displacement amplifier integrated into compliant XY positioner.

The XY positioner has the capability of conducting vibrations either individually or simultaneously through the utilization of two PZT actuators in two perpendicular orientations, as shown in Figure 2. In addition, the XY stage comprises an eight-lever displacement amplification mechanism, a parallel guiding mechanism, and a central platform, as illustrated in Figure 2. More specifically, the parallel guiding mechanism utilizes right circular hinges and rigid joints to decline parasitic motion error and increase the stiffness of the proposed positioner. The main dimensions of the platform are demonstrated in Figure 3. In addition, the key dimension values of the developed positioner with dimension units of mm are illustrated in Table 1. The total dimensions of the suggested positioner were $204 \times 204 \times 15$ (mm).

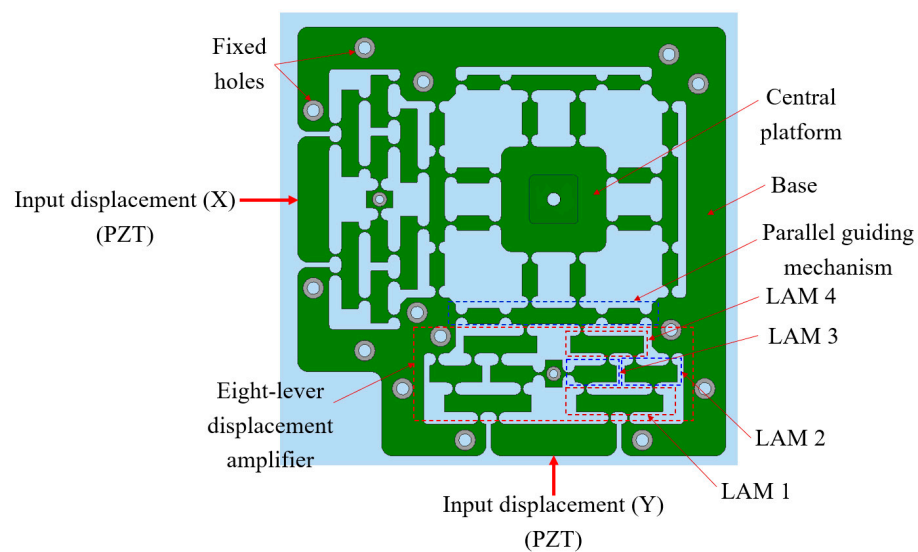


Figure 2. Proposed design for compliant XY positioner.

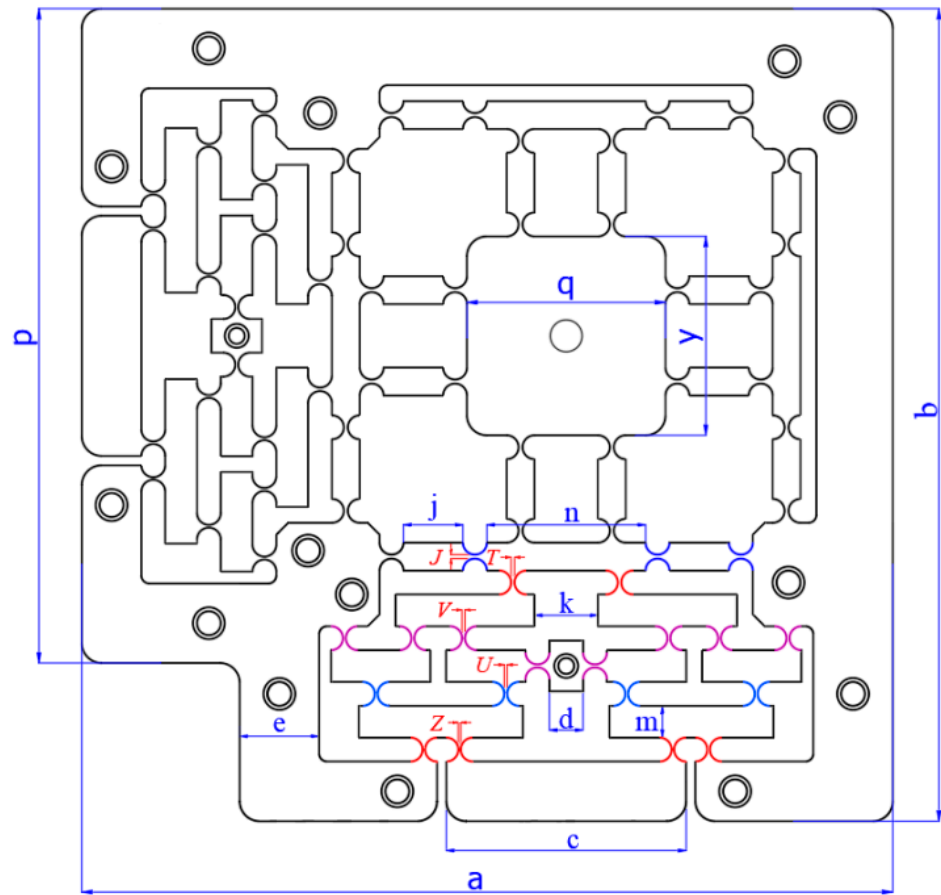


Figure 3. Diagram illustrating the key dimensions of the developed positioner.

Table 1. Important factors of the suggested platform (unit: mm).

Symbolization	Value	Symbolization	Value
a	204	p	164
b	204	q	50
c	60	y	50
d	8.5	x	94
e	20	J	$0.5 < J < 0.7$
m	8	T	$0.6 < T < 0.8$
n	40	V	$0.7 < V < 0.9$
k	16	U	$0.8 < U < 1$
j	15	Z	$1 < Z < 1.2$

3. Proposed Hybrid Method

The stage has been constructed to adhere to the eight-lever displacement amplifier, incorporating circular hinges. The dynamic equations of the positioner were obtained through an analytical investigation utilizing the PRBM and Lagrange methods. Subsequently, based on the theoretical equations, the Crayfish optimization technique was utilized to optimize the crucial variables of the produced positioner to improve the stage's quality response. More details about the Crayfish optimization algorithm can be read in the ref. [29]. Figure 4 depicts the flowchart of the suggested optimal strategy for the developed positioner. The following is a concise summary of the proposed hybrid approach.

- Develop a conceptual design for the positioner that aligns with the desired output response and technical performances.
- Build analytical equations for the XY positioner based on the pseudo-rigid-body model (PRBM) and Lagrange's methodology.

- Validate the analytical findings by the finite element method (FEM).
- The application of the mathematical model for subsequent optimization processes is contingent upon the correction of the analytical equations.
- A determination is made regarding the key parameters, constraint function, as well as the objective function.
- The Crayfish optimization algorithm is utilized for optimizing the main design variables of the proposed stage.
- Manufacture the prototype of the developed XY stage.
- The verification of optimal outcomes is conducted through simulations using ANSYS software 19.2 and experimental methods.

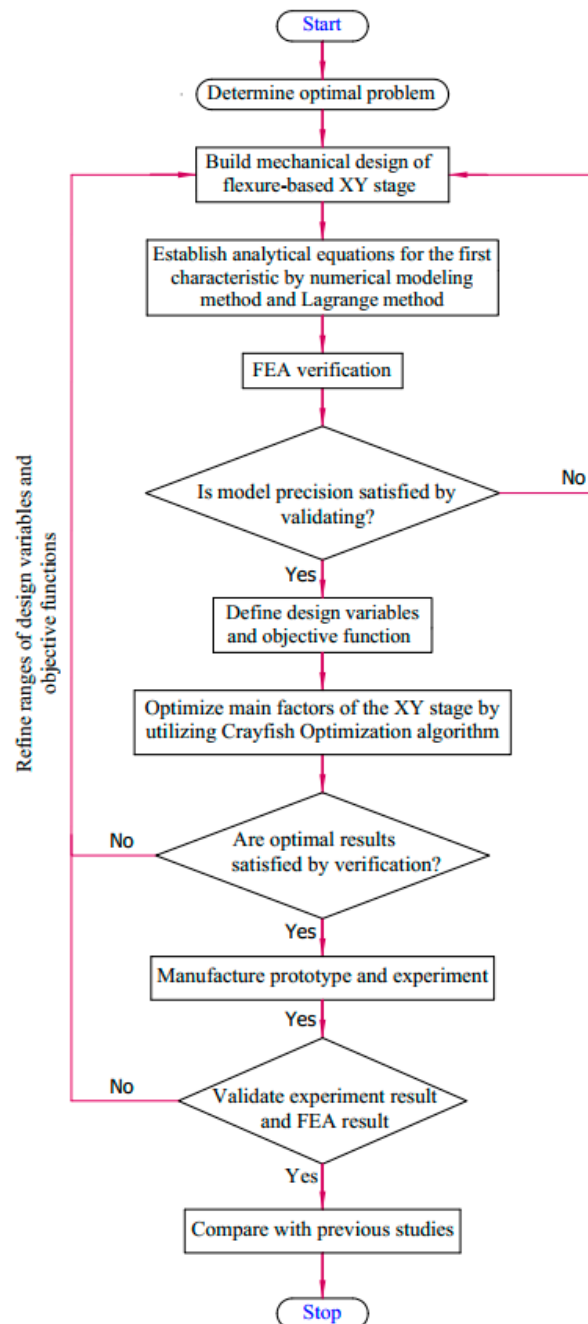


Figure 4. Diagram illustrating the proposed optimization hybrid technique for an XY positioner.

4. Results and Discussion

4.1. Enhanced Positioning Mechanism with Dynamic Formation

The dynamic modeling of the recommended positioner is developed by utilizing the PRBM methodology and Lagrange technique. The acquired consequences are confirmed through the application of the FEM. Figure 5 depicts a schematic representation of the PRBM design for the positioner.

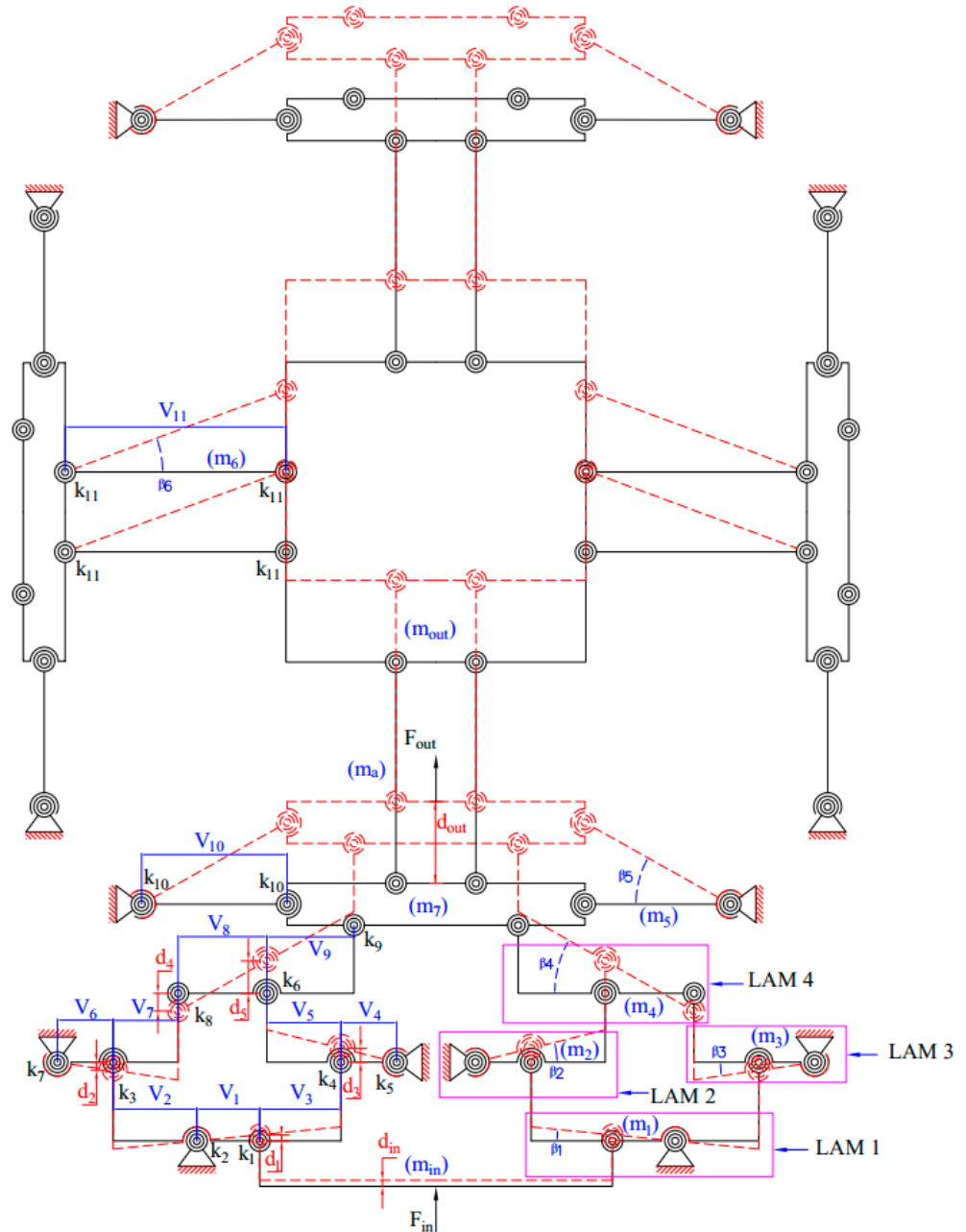


Figure 5. An architecture for modeling the vibration-integrated compliant platform using PRBM method.

This research proposes an integration of right circular hinges into a new developed positioner to improve the stiffness and initial natural frequency of the stage. As illustrated in Figure 6, the key parameters of the utilized flexure hinge are the thickness (t_c) and radius (r) of the right circular hinge, as well as its width (b_c).

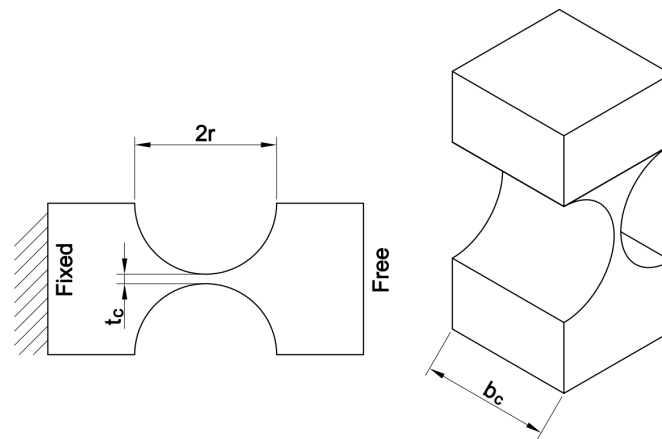


Figure 6. Main parameters of right circular hinge.

The input and output displacements of the displacement amplifier are denoted as d_{in} and d_{out} , correspondingly, as depicted in Figures 2 and 5. The input displacement of the second floor, as well as the third floor, is equivalent to the output displacement of the first floor. Furthermore, the output of the second and third floors serves as the input displacement for the fourth floor. The stage’s dynamic equation is derived from a series of equations.

$$d_{in} \frac{V_2}{V_1} = d_2 \tag{1}$$

$$d_{in} \left(\frac{V_1 + V_3}{V_1} \right) = d_3 \tag{2}$$

$$d_2 \left(\frac{V_6 + V_7}{V_6} \right) = d_4 \tag{3}$$

$$d_3 \left(\frac{V_4 + V_5}{V_4} \right) = d_5 \tag{4}$$

$$\begin{aligned} d_{out} &= d_4 \frac{V_9}{V_8} + d_5 \left(\frac{V_8 + V_9}{V_8} \right) = d_2 \left(\frac{V_9(V_6 + V_7)}{V_6 V_8} \right) + d_3 \left(\frac{(V_4 + V_5)(V_8 + V_9)}{V_4 V_8} \right) \\ &= d_{in} \left(\frac{V_2 V_9 (V_6 + V_7)}{V_1 V_6 V_8} \right) + d_{in} \left(\frac{(V_1 + V_3)(V_4 + V_5)(V_8 + V_9)}{V_1 V_4 V_8} \right) \end{aligned} \tag{5}$$

$$AR = \frac{d_{out}}{d_{in}} = \frac{V_2 V_4 V_9 (V_6 + V_7) + V_6 (V_1 + V_3)(V_4 + V_5)(V_8 + V_9)}{V_1 V_4 V_6 V_8} \tag{6}$$

where the variable m_i symbolizes the mass, V_i indicates the distance and β_i ($i = 1, 2, \dots, 9, 10$) signifies the rotating angles of the stiff links. Furthermore, Equation (7) provides a description of the torsion stiffness (K_i) of the circular joint, whereas Equation (8) describes the inertia moment (I_i) of the rigid-linkages.

$$K_i = \frac{2Eb_i t_i^{2.5}}{9\pi r_i^{0.5}} \tag{7}$$

$$I_i = \frac{m_i L_i^2}{12} \tag{8}$$

where E , b_i , t_i , r_i are the Young modulus, width, thickness and radius of right circular hinges.

Equation (9) illustrates the definition of the kinetic energy associated with the developed positioner.

$$E_k = \sum_{i=1}^6 (E_t + E_r) = \sum_{i=1}^6 \left(\frac{1}{2} m_i v_i^2 + \frac{1}{2} I_i \dot{\beta}_i^2 \right) \tag{9}$$

The kinetic energy of every rigid-link is computed using Equation (10).

$$\begin{aligned}
E_k = & \frac{1}{2}m_{in}\left(\frac{V_1}{2}\dot{\beta}_1\right)^2 + \frac{1}{2}m_1\left(\frac{V_1+V_2+V_3}{2}\dot{\beta}_1\right)^2 + \frac{1}{2}I_1\dot{\beta}_1^2 + \frac{1}{2}m_2\left(\frac{V_4+V_5}{2}\dot{\beta}_2\right)^2 \\
& + \frac{1}{2}I_2\dot{\beta}_2^2 + \frac{1}{2}m_3\left(\frac{V_6+V_7}{2}\dot{\beta}_3\right)^2 + \frac{1}{2}I_3\dot{\beta}_3^2 + \frac{1}{2}m_4\left(\frac{V_8+V_9}{2}\dot{\beta}_4\right)^2 + \frac{1}{2}I_4\dot{\beta}_4^2 \\
& + \frac{1}{2}m_5\left(\frac{V_{10}}{2}\dot{\beta}_5\right)^2 + \frac{1}{2}I_5\dot{\beta}_5^2 + \frac{1}{2}m_6\left(\frac{V_{11}}{2}\dot{\beta}_6\right)^2 + \frac{1}{2}I_6\dot{\beta}_6^2 + \frac{1}{4}m_7\left(\frac{V_8+V_9}{2}\dot{\beta}_4\right)^2 \\
& + \frac{1}{4}m_{out}\left(\frac{V_8+V_9}{2}\dot{\beta}_4\right)^2 + \frac{1}{2}m_a\left(\frac{V_8+V_9}{2}\dot{\beta}_4\right)^2
\end{aligned} \quad (10)$$

The equation that defines the elastic energy of the structure seen in Figure 5 is as follows:

$$E_v = \sum_{i=1}^6 \frac{1}{2} K_j \beta_i^2 \quad (11)$$

Elastic energy is provided by the deformation of the right circular hinge.

$$\begin{aligned}
E_v = & \frac{1}{2}(K_1 + K_2 + K_3 + K_4)\beta_1^2 + \frac{1}{2}(K_5 + K_6)\beta_2^2 \\
& + \frac{1}{2}(K_7 + K_8)\beta_3^2 + \frac{1}{2}K_9\beta_4^2 + \frac{1}{2}2K_{10}\beta_5^2 + \frac{1}{2}4K_{11}\beta_6^2
\end{aligned} \quad (12)$$

The equations provided involve the variables $(\beta_i, \dot{\beta}_i)$, which represent the rotational angular velocity and angular velocity of each link. The interconnections between rotary angulars can be approximated by a series of equations.

$$\beta_1 = \frac{d_{in}}{V_1} \quad (13)$$

$$\beta_2 = \left(\frac{V_2}{V_6 + V_7}\right)\beta_1 \quad (14)$$

$$\beta_3 = \left(\frac{V_1 + V_3}{V_4 + V_5}\right)\beta_1 \quad (15)$$

$$\beta_4 = \left(\frac{V_2V_4V_9(V_6 + V_7) + V_6(V_1 + V_3)(V_4 + V_5)(V_8 + V_9)}{V_4V_6V_8(V_8 + V_9)}\right)\beta_1 \quad (16)$$

$$\beta_5 = \left(\frac{V_2V_4V_9(V_6 + V_7) + V_6(V_1 + V_3)(V_4 + V_5)(V_8 + V_9)}{V_4V_6V_8V_{10}}\right)\beta_1 \quad (17)$$

$$\beta_6 = \left(\frac{V_2V_4V_9(V_6 + V_7) + V_6(V_1 + V_3)(V_4 + V_5)(V_8 + V_9)}{V_4V_6V_8V_{11}}\right)\beta_1 \quad (18)$$

For the input force F_{in} , the work can be calculated as:

$$W = \frac{1}{2}F_{in}d_{in} \quad (19)$$

Given the equation $W = E_v$, it is possible to derive the relationship between the input displacement and input force.

$$\frac{1}{2}F_{in}d_{in} = \frac{1}{2} \left[\begin{aligned} & (K_1 + K_2 + K_3 + K_4)\frac{1}{V_1^2} + (K_5 + K_6)\left(\frac{V_2}{V_1(V_6+V_7)}\right)^2 \\ & + (K_7 + K_8)\left(\frac{V_1+V_3}{V_1(V_4+V_5)}\right)^2 \\ & + K_9\left(\frac{V_2V_4V_9(V_6+V_7)+V_6(V_1+V_3)(V_4+V_5)(V_8+V_9)}{V_1V_4V_6V_8(V_8+V_9)}\right)^2 \\ & + 2K_{10}\left(\frac{V_2V_4V_9(V_6+V_7)+V_6(V_1+V_3)(V_4+V_5)(V_8+V_9)}{V_1V_4V_6V_8V_{10}}\right)^2 \\ & + 4K_{11}\left(\frac{V_2V_4V_9(V_6+V_7)+V_6(V_1+V_3)(V_4+V_5)(V_8+V_9)}{V_1V_4V_6V_8V_{11}}\right)^2 \end{aligned} \right] d_{in}^2 \quad (20)$$

To determine the stiffness of the mechanism, we define the input stiffness as $K_{in} = F_{in}/d_{in}^2$ and divide the parts equally by d_{in}^2 .

$$\begin{aligned}
 K_{in} = & (K_1 + K_2 + K_3 + K_4) \frac{1}{V_1^2} + (K_5 + K_6) \left(\frac{V_2}{V_1(V_6+V_7)} \right)^2 \\
 & + (K_7 + K_8) \left(\frac{V_1+V_3}{V_1(V_4+V_5)} \right)^2 \\
 & + K_9 \left(\frac{V_2 V_4 V_9 (V_6+V_7) + V_6 (V_1+V_3) (V_4+V_5) (V_8+V_9)}{V_1 V_4 V_6 V_8 (V_8+V_9)} \right)^2 \\
 & + 2K_{10} \left(\frac{V_2 V_4 V_9 (V_6+V_7) + V_6 (V_1+V_3) (V_4+V_5) (V_8+V_9)}{V_1 V_4 V_6 V_8 V_{10}} \right)^2 \\
 & + 4K_{11} \left(\frac{V_2 V_4 V_9 (V_6+V_7) + V_6 (V_1+V_3) (V_4+V_5) (V_8+V_9)}{V_1 V_4 V_6 V_8 V_{11}} \right)^2
 \end{aligned} \tag{21}$$

The structure can store kinetic energy (E_k) and elastic energy (E_v). The Lagrange function $L = E_k - E_v$ can be obtained by substituting the kinetic and elastic energy.

$$L = E_k - E_v \tag{22}$$

$$\sum_{i=1}^6 \left\{ \frac{d}{dt} \left(\frac{\partial L}{\partial \dot{\beta}_i} \right) - \frac{\partial L}{\partial \beta_i} = Q_i \right\} \tag{23}$$

The definition of the equation of motion is expressed as

$$\bar{M} \ddot{\beta}_1 + \bar{K} \dot{\beta}_1 = 0, \tag{24}$$

in which:

$$\begin{aligned}
 \bar{M} = & m_{in} \left(\frac{V_1}{2} \right)^2 + m_1 \left(\frac{V_1+V_2+V_3}{2} \right)^2 + I_1 \\
 & + m_2 \left(\frac{V_2(V_4+V_5)}{2(V_6+V_7)} \right)^2 + I_2 \left(\frac{V_2}{V_6+V_7} \right)^2 \\
 & + m_3 \left(\frac{(V_6+V_7)(V_1+V_3)}{2(V_4+V_5)} \right)^2 + I_3 \left(\frac{V_1+V_3}{V_4+V_5} \right)^2 \\
 & + m_4 \left(\frac{V_2 V_4 V_9 (V_6+V_7) + V_6 (V_1+V_3) (V_4+V_5) (V_8+V_9)}{2V_4 V_6 V_8} \right)^2 \\
 & + I_4 \left(\frac{V_2 V_4 V_9 (V_6+V_7) + V_6 (V_1+V_3) (V_4+V_5) (V_8+V_9)}{V_4 V_6 V_8 (V_8+V_9)} \right)^2 \\
 & + 2m_5 \left(\frac{V_2 V_4 V_9 (V_6+V_7) + V_6 (V_1+V_3) (V_4+V_5) (V_8+V_9)}{2V_4 V_6 V_8} \right)^2 \\
 & + 2I_5 \left(\frac{V_2 V_4 V_9 (V_6+V_7) + V_6 (V_1+V_3) (V_4+V_5) (V_8+V_9)}{V_4 V_6 V_8 V_{10}} \right)^2 \\
 & + 2m_6 \left(\frac{V_2 V_4 V_9 (V_6+V_7) + V_6 (V_1+V_3) (V_4+V_5) (V_8+V_9)}{2V_4 V_6 V_8} \right)^2 \\
 & + 2I_6 \left(\frac{V_2 V_4 V_9 (V_6+V_7) + V_6 (V_1+V_3) (V_4+V_5) (V_8+V_9)}{V_4 V_6 V_8 V_{11}} \right)^2 \\
 & + m_7 \left(\frac{V_2 V_4 V_9 (V_6+V_7) + V_6 (V_1+V_3) (V_4+V_5) (V_8+V_9)}{2V_4 V_6 V_8} \right)^2 \\
 & + \frac{1}{2} m_{out} \left(\frac{V_2 V_4 V_9 (V_6+V_7) + V_6 (V_1+V_3) (V_4+V_5) (V_8+V_9)}{2V_4 V_6 V_8} \right)^2 \\
 & + 2m_a \left(\frac{V_2 V_4 V_9 (V_6+V_7) + V_6 (V_1+V_3) (V_4+V_5) (V_8+V_9)}{2V_4 V_6 V_8} \right)^2,
 \end{aligned} \tag{25}$$

$$\begin{aligned}
\bar{K} = & 2(K_1 + K_2 + K_3 + K_4) + 2(K_5 + K_6) \left(\frac{V_2}{V_6 + V_7} \right)^2 + 2(K_7 + K_8) \left(\frac{V_1 + V_3}{V_4 + V_5} \right)^2 \\
& + 2K_9 \left(\frac{V_2 V_4 V_9 (V_6 + V_7) + V_6 (V_1 + V_3) (V_4 + V_5) (V_8 + V_9)}{V_4 V_6 V_8 (V_8 + V_9)} \right)^2 \\
& + 8K_{10} \left(\frac{V_2 V_4 V_9 (V_6 + V_7) + V_6 (V_1 + V_3) (V_4 + V_5) (V_8 + V_9)}{V_4 V_6 V_8 V_{10}} \right)^2 \\
& + 8K_{11} \left(\frac{V_2 V_4 V_9 (V_6 + V_7) + V_6 (V_1 + V_3) (V_4 + V_5) (V_8 + V_9)}{V_4 V_6 V_8 V_{11}} \right)^2.
\end{aligned} \tag{26}$$

From the above formulations, the resonant frequency of the developed XY stage is yielded as below.

$$f = \frac{1}{2\pi} \left(\frac{\bar{K}}{\bar{M}} \right)^{0.5} \tag{27}$$

4.2. Validation of the Formed Theory Modelling

The validity of the theoretical findings was confirmed through the utilization of FEA analysis. The natural frequency, as per the theory, was determined to be 990.74 Hz. Initially, the stage's 3D model was built using a rough mesh. Next, in order to improve the accuracy of the calculations, the mesh of the model was purified at the specific points where the circular hinges were located, as seen in Figure 7. Later, the Skewness criteria were employed to evaluate the mesh's quality. More details about mathematical equations to evaluate the mesh quality for different mesh element kinds based on the Skewness criteria can be read in the ref. [30]. The attained consequence of a moderate worth based on this benchmark was 0.35865, as depicted in Figure 8. This value ensured the achievement of an exemplary mesh for the simulated procedure of the developed stage. The result obtained by using the Finite Element Method (FEM) showed that the first resonant frequency was calculated to be at 1058.5 Hz, as depicted in Figure 9.

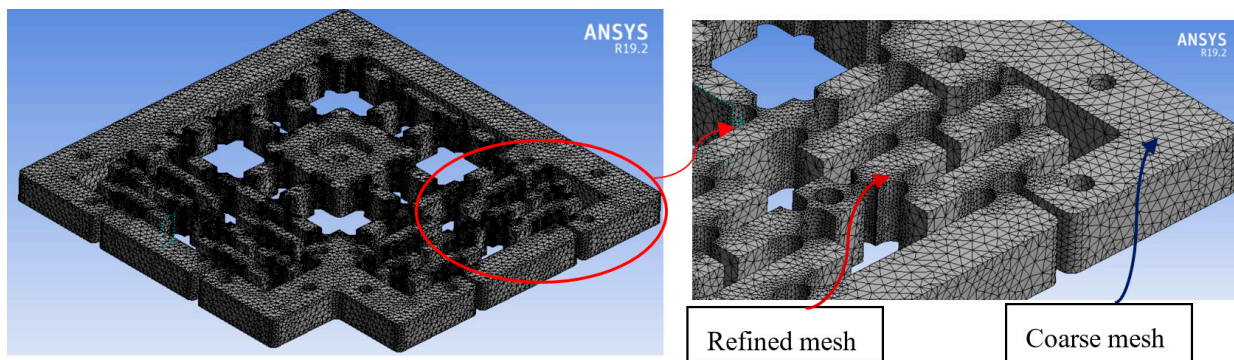


Figure 7. Meshing model for proposed positioner.

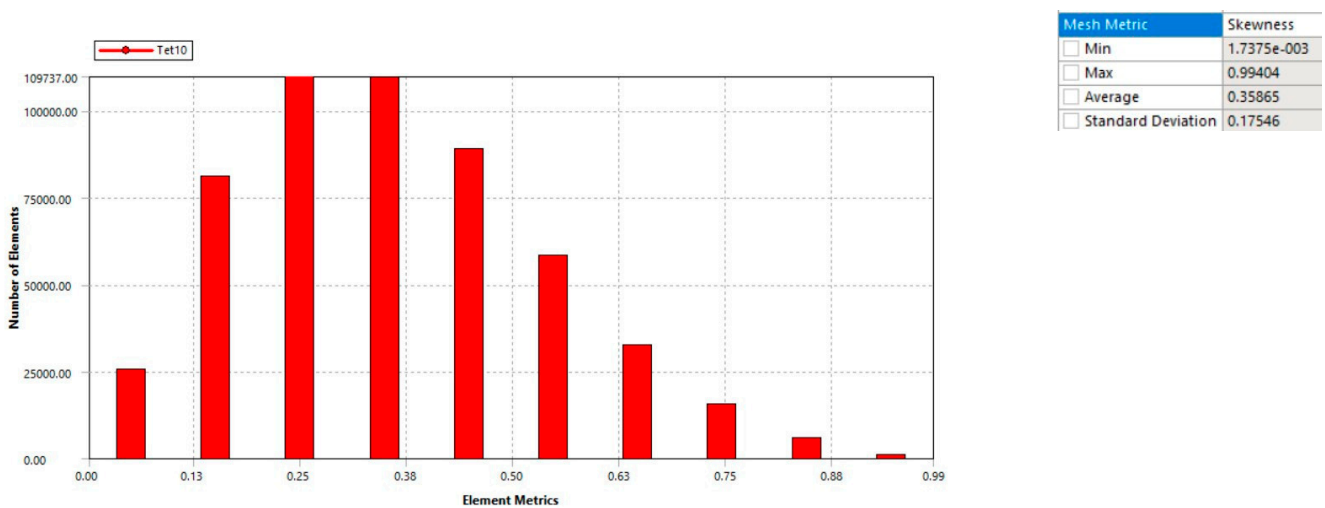


Figure 8. The meshing quality of the suggested positioner based on Skewness criteria.

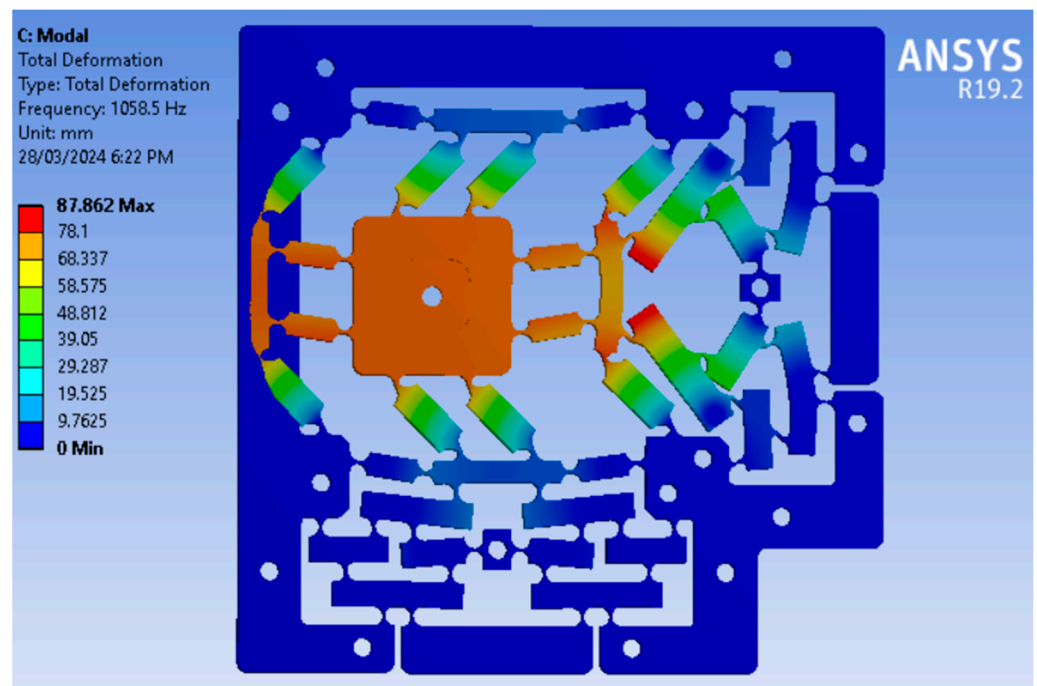


Figure 9. The first resonant frequency according to FEA analysis.

The inaccuracy between the theoretical and FEM methods, as indicated in Table 2, is around 6.4%. This implies that the devised modeling technique is sufficient for assessing the output attribute of the positioner.

Table 2. Verification of the analytical outcome vs. FEM consequence.

Attribute	Analytical	FEM	Inaccuracy (%)
f (Hz)	990.74	1058.5	6.4

4.3. Factor Optimization of 02 Dof Stage

The first step was the establishment of an analytical model for the proposed stage, which was designed to assess the quality response using the PRBM method and Lagrange method. The vibration-assisted stage was configured in a parallel manner, with each

direction (X as well as Y) being engaged independently. An analysis of a single direction is adequate for the entire design because of its symmetrical structure. In order to mitigate the occurrence of resonance phenomena between the PEA actuator and the developed positioner, the first natural frequency modes were either limited or enhanced. To enhance the prompt reactivity of the positioners, it is advisable to select the initial natural frequency with the maximum feasible magnitude. Furthermore, it can be observed that the angular frequency exhibits a direct relationship with the natural frequency of the compliant stage. Hence, it is recommended to optimize the first natural frequency in order to improve the response speed and mitigate the phenomenon of resonance in the positioner. The key aim of this research is to enhance the resonance frequency, whereby it is concisely defined as.

Seek the total variable: $\mathbf{X} = [Z, U, V, T, J]$

$$\text{Maximize } f(\mathbf{X}), \quad (28)$$

S.t:

$$f(X) > 1100 \text{ Hz}, \quad (29)$$

Limitations of main parameters (unit: mm):

$$\begin{cases} 0.5 \leq J \leq 0.7 \\ 0.6 \leq T \leq 0.8 \\ 0.7 \leq V \leq 0.9 \\ 0.8 \leq U \leq 1 \\ 1 \leq Z \leq 1.2 \end{cases}, \quad (30)$$

where $f(\mathbf{X})$ symbolizes the resonant frequency. In addition, the main design variables Z , U , V , and T denote the thickness of right circular hinges on the first floor, second floor, third floor and fourth floor, respectively. Furthermore, the thickness of the circular hinge on the guiding mechanism is noted by J .

The variety of design variations is contingent upon the design experiences and the specific attributes of various floors. Expressly, it is recommended that the thicknesses of floors are different in order to avoid a loss of the motion energy. Furthermore, the thickness of the flexure hinges in the second stage is greater than the thickness of the flexure hinges on the third stage, and the thickness of the hinges on the 3rd stage should be greater than the thickness of the hinges in the fourth stage.

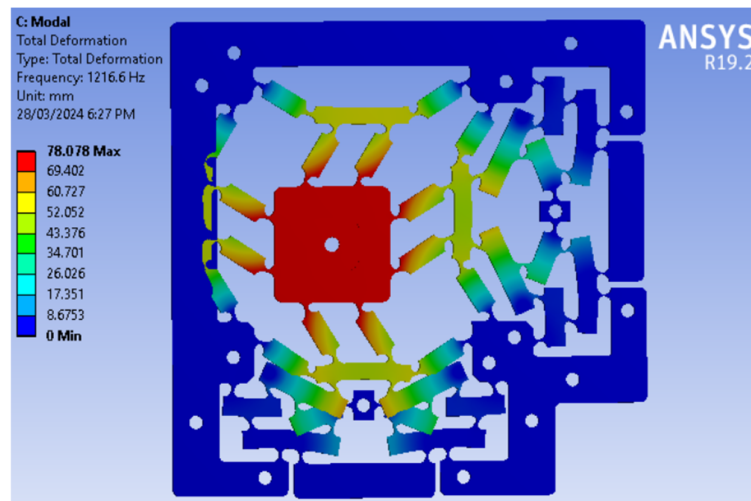
It is necessary for ensuring the suggested positioner's robustness while also minimizing the dissipation of displacement energy. To achieve the maximum value for the designed mechanism, it is vital to determine the appropriate thickness of distinct places on various floors through the utilization of an optimization technique.

MATLAB R2021b was used for building the combination strategy of the PRBM methodology and Lagrange's method, as well as the Crayfish optimization algorithm, based on Equations (1)–(30). Consequently, the stage's ideal parameters were determined to be $J = 0.7$ mm; $T = 0.8$ mm; $V = 0.9$ mm; $U = 1$ mm; and $Z = 1.2$ mm. These findings indicated that the estimated value for the first frequency is around 1232.65 Hz.

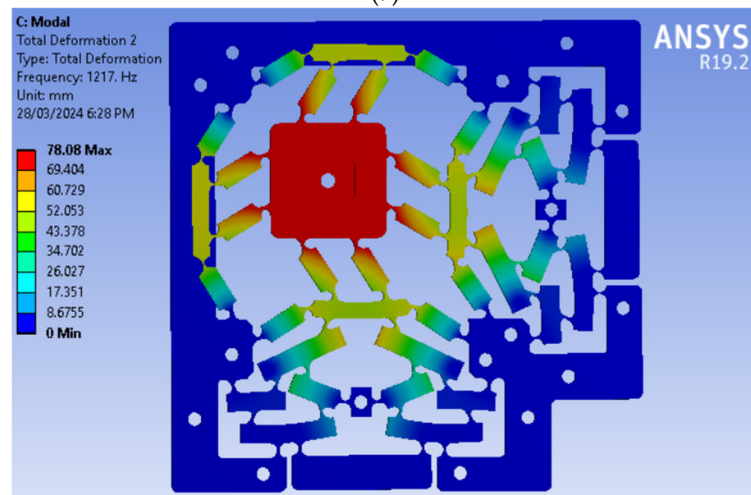
The optimal outcome was confirmed using the FEM method. The optimal parameters were specifically employed to construct a 3D model for the purpose of verifying the optimal outcome. The obtained results indicated that the first resonant frequency, as determined by the FEA analysis, was 1216.6 Hz, as depicted in Figure 10a. Additionally, an inaccuracy between the optimal consequence and the FEA consequence was 1.32%, as exhibited in Table 3. Furthermore, based on optimal results, the frequency values of the stage obtained from the first natural modes using the FEM method were determined to be at 1216.6 Hz, 1217 Hz, 1910.9 Hz, 1962.5 Hz, 2810.1 Hz, and 2814.1 Hz, respectively, as depicted in Figure 10a–f. In addition, based on FEA results, the workspace of the structure probed in the X and Y directions with a safety factor of higher than 1.8 was 35.096×35.188 (μm).

Table 3. Confirmation for the optimal consequence according to FEM consequence.

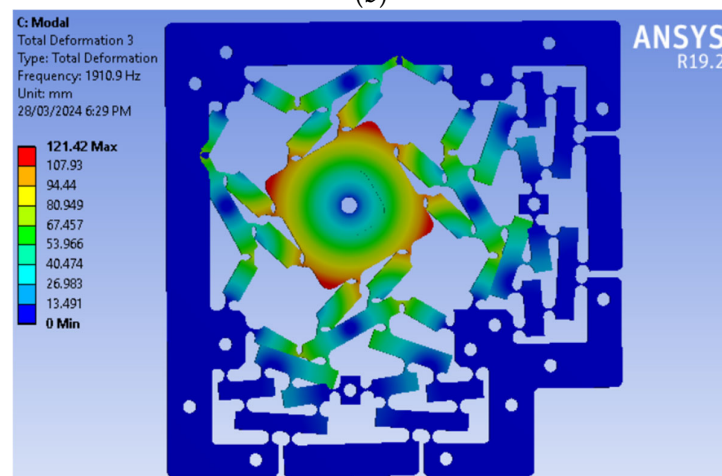
Attribute	Optimal Result	FEM Result	Imprecision (%)
f (Hz)	1232.65	1216.6	1.32



(a)



(b)



(c)

Figure 10. Cont.

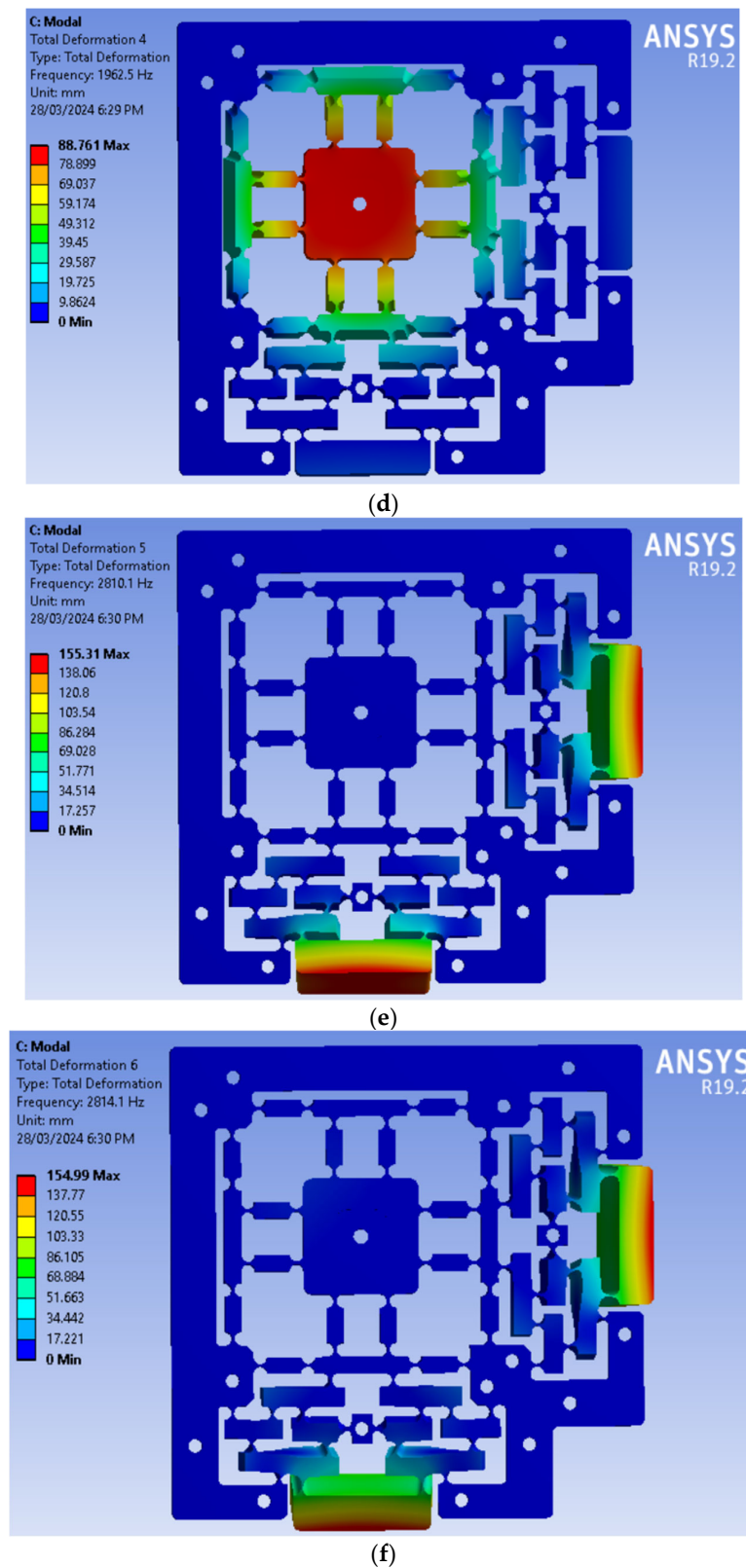


Figure 10. Optimal results of resonant frequencies at six modes based on FEA analysis. (a) The natural frequency of the first mode. (b) The natural frequency of the second mode. (c) The natural frequency of the third mode. (d) The natural frequency of the fourth mode. (e) The natural frequency of the fifth mode. (f) The natural frequency of the sixth mode.

4.4. Experimental Results

4.4.1. Assessment of the 1st Natural Frequency

The configuration of the experiment, as depicted in Figure 11, was designed to assess the analytical and simulated calculations of the dynamic characteristic of the structure. The LK-G30 laser displacement sensor, manufactured by Keyence (Osaka, Japan), accurately measured the vibration of the center stage in the X and Y directions with a precision of $0.05\ \mu\text{m}$. The first resonant frequency of the stage was determined using the hammer test method, which involved analyzing the recorded data from a laser sensor LK-G30. The laser displacement sensor was controlled by software. Subsequently, the collected data were subjected to analysis via the rapid Fourier transform algorithm implemented in the Matlab software R2021b. The experimental result was depicted in Figure 12, and the initial crest of the frequency spectrum was observed at 1127.62 Hz. Furthermore, the obtained outcome demonstrated a 7.31% disparity between the FEA outcome and the experimental outcome, as given in Table 4. Consequently, the error was minor and closely aligned with the FEA outcome.

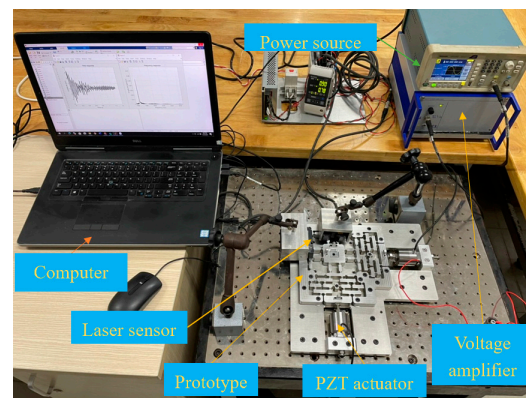


Figure 11. Experiment installation for measuring the first natural frequency.

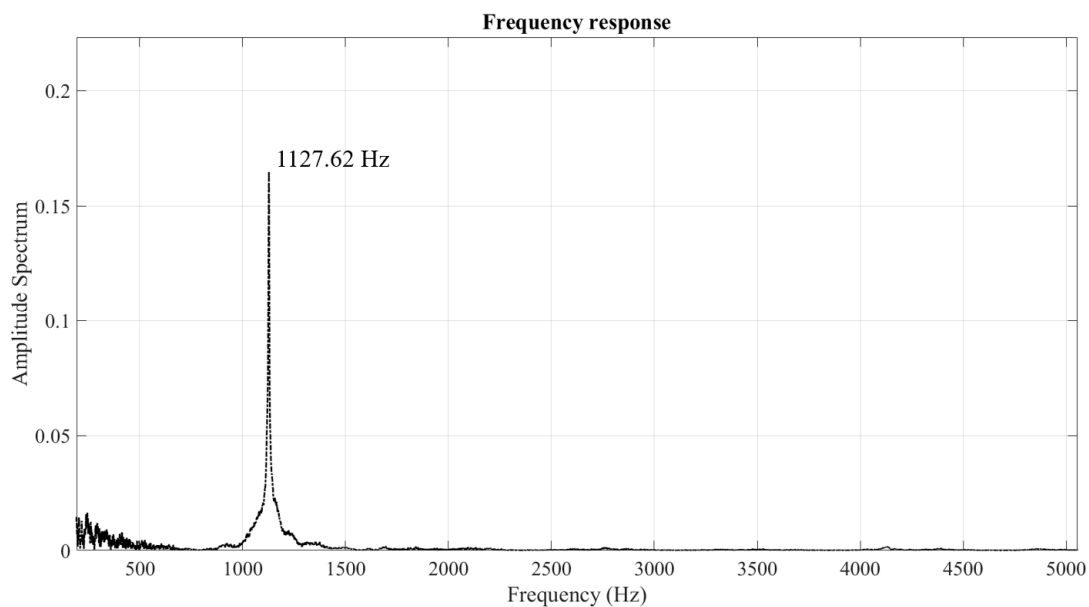


Figure 12. The experimental first natural frequency.

Table 4. Confirmation for the experimental consequence and FEA consequence.

Characteristic	FEA Result	Experimental Result	Imprecision (%)
f (Hz)	1216.6	1127.62	7.31

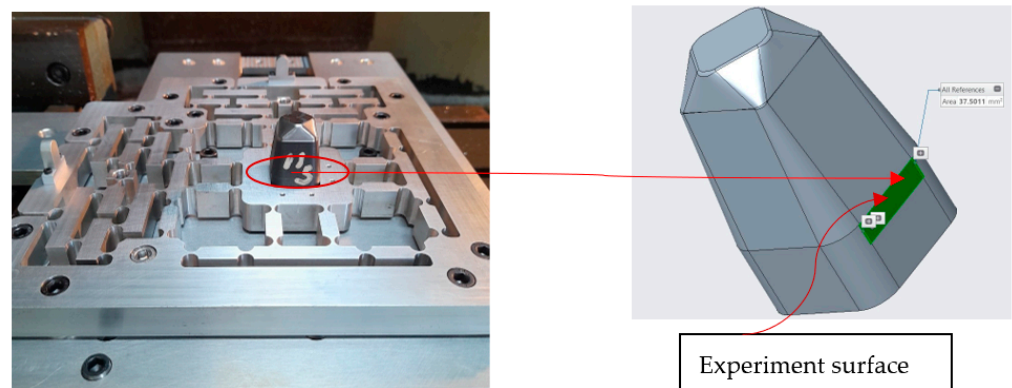
Moreover, the first natural frequency of optimal design comparing initial design according to the FEM method was enhanced 14.94%, as depicted in Table 5.

Table 5. First natural frequency enhancement of optimal design vs. initial design.

Response	Initial Result	Optimal Result	Enhancement (%)
f (Hz)	1058.5	1216.6	14.94

4.4.2. Investigation of Experimental Fine CNC Milling on Prototype

The configuration of the experiment, depicted in Figure 13, was constructed to facilitate the fabrication of side face CNC milling tests. The primary objective of this setup was to expedite the assessment of the attribute of the proposed combination manufacturing technique in comparison to the conventional CNC milling procedure. The fabricating procedure in this experiment is implemented using the CNC milling device, namely VMC-650 (Huey Long, Taichung, Taiwan). The specimen material is a hardness material, namely 2083, applied for fabricating plastic mold. The vibration milling equipment with aided motion could operate in two directions, either independently or concurrently. These instructions adhere to the feed directions in both the X and Y dimensions. The key objective of this experiment is to examine the influence of vibration frequency on the feed path by employing a PEA actuator. In addition, the purpose is to compare the surface roughness of fabricated specimens produced using non-vibration manufacturing versus assisted vibration manufacturing methods.

**Figure 13.** The fabricated surface for experimental specimen.

This experiment was conducted with fixed cutting conditions such as a spindle speed of 2000 rpm, a feed rate of 200 mm/min, a cutting thickness of 0.03 mm, a milling tool diameter of 6 mm, and a dry cutting condition. In addition, the vibration frequency with a maximum voltage of 10 V based on a PEA actuator with a maximal travel of 15 μm was checked with four grades (700 Hz, 800 Hz, 900 Hz and 1000 Hz). Furthermore, a frequency producer called an AFG1022 (Tektronix, Beaverton, OR, USA) supplied the natural frequency for both PEA motors, namely P-225.10 (PI manufacturer: a German company, Karlsruhe, Germany), to facilitate vibration in the CNC milling process. This was conducted to examine the quality response of the fabricated specimen, as depicted in Figure 14. The experimental installation for checking the surface roughness of the side faces of the fabricated specimen was depicted in Figure 15. In addition, the surface roughness of the specimen was evaluated by a roughness surface tester, namely Accretech, Japan. The results of the experiment are demonstrated in Table 6. The attained results showed

that the values for surface roughness at 800 Hz and 900 Hz were better than the results at 700 Hz and 1000 Hz. The best surface roughness achieved a Ra of 0.287 μm with a provided frequency of 900 Hz. Therefore, the assisted vibration CNC milling method enhanced the surface roughness of the specimen in a suitable frequency range.

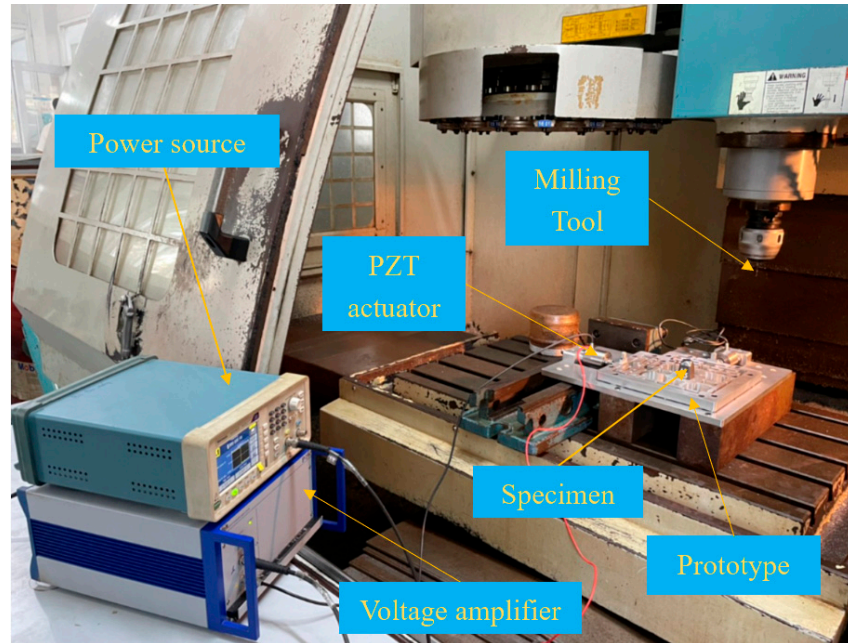


Figure 14. Vibration-assisted CNC milling installation based on a PZT actuator.

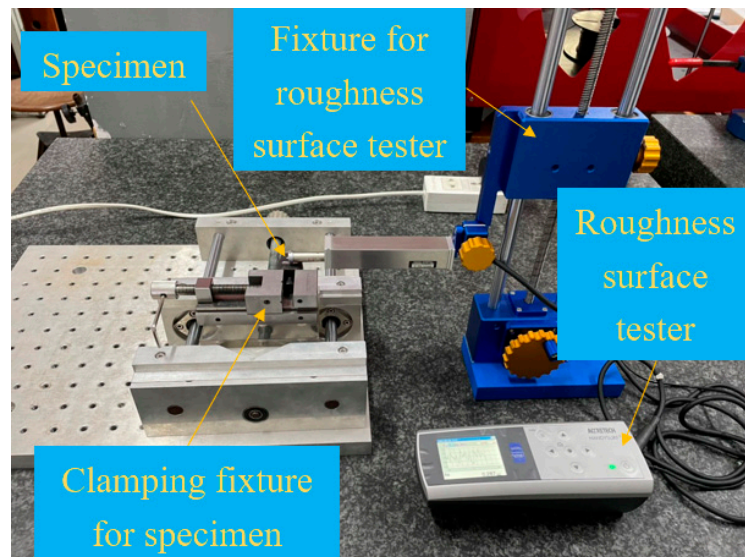


Figure 15. The experimental installation for checking the surface roughness of fabricated side faces.

Table 6. Assisted vibration CNC milling experiments.

No.	Frequency (Hz)	Surface Roughness (μm) Measured by Assisted Vibration CNC Milling	Surface Roughness (μm) Measured by Traditional Fabrication Method
1	700 Hz	0.359	0.321
2	800 Hz	0.307	0.321
3	900 Hz	0.287	0.321
4	1000 Hz	0.68	0.321

Table 7 presents a relationship between the current design and various other previous structures.

Table 7. Examining the present positioner in relation to prior positioners.

Research	Total Measurements	1st Natural Frequency (Hz)
Lai et al. [31]	N/A	181.29
Gu et al. [20]	N/A	411.23
Pham et al. [23]	340 mm × 340 mm	692.7
The developed positioner	204 mm × 204 mm	1127.62

The findings indicate that the current positioner has a greater initial natural frequency than previous positioners. More specifically, Pham et al. [23] developed the XY stage for the vibration-assisted CNC milling process with an investigated specimen of AL6061 with a minimal surface roughness of 1.13 μm and an experiment frequency of 325 Hz. This research developed a new XY positioner with an investigated hard specimen of 2083 with a best surface roughness of 0.287 μm at an experiment frequency of 900 Hz.

5. Conclusions

A novel design of an XY positioner for vibration-assisted CNC milling is presented in this research. The development of this mechanism was based on the integration of right circular hinges with an eight-lever displacement amplifier. The authors suggested a hybrid technique that combines the pseudo-rigid-body model with the Lagrange method, finite element method, and Crayfish optimization algorithm for improving the output characteristic of the enhanced mechanism. This strategy aims to optimize the key parameters of the developed stage. The initial step involved the establishment of analytical equations based on the PRBM and Lagrange approach so as to establish the key response of the developed positioner. The achieved finding indicated that the analytical value for the first natural frequency was determined to be 990.74 Hz. Subsequently, the accuracy of the model was confirmed using FEA analysis. The FEA result yielded a first natural frequency of 1058.5 Hz with a 6.4% inaccuracy among the theoretical approach and the FEA analysis. Hence, the error was minimal and deemed dependable for the subsequent optimization procedure.

Next, the Crayfish optimization technique was utilized to optimize the key design variables of the developed stage with the aim of improving the quality response, as indicated by the formed equations chain. The optimization findings obtained indicated that the stage's optimal parameters were $J = 0.7$ mm, $T = 0.8$ mm, $V = 0.9$ mm, $U = 1$ mm, and $Z = 1.2$ mm, and the optimal value of first natural frequency was 1232.65 Hz. Furthermore, the ideal outcome was confirmed by FEA analysis. The optimal key factors were employed to construct a 3D design in order to verify the optimal result based on the FEM method. The FEA analysis yielded an optimal result of 1216.6 Hz with a 1.32% error between the optimal result obtained by the analytical technique and the FEA method.

Furthermore, the experimental procedure was carried out in order to validate the ideal outcome derived from the FEM method. The obtained results indicated that the experimental value was 1127.62 Hz and the deviation between the optimal value obtained through FEA analysis and the experimental technique was 7.31%. The error was discovered and resolved by FEA analysis. A machining experiment was conducted to showcase the benefits of vibration-assisted milling compared to conventional milling methods, particularly in relation to surface roughness standards. The experimental procedure involved the manipulation of vibration frequencies within the range of 700 to 1000 Hz. The results demonstrated an enhancement in surface roughness, specifically during the frequency range of 800 Hz to 900 Hz. Nevertheless, the surface quality exhibited a decline as the frequency was elevated within the values of 700 Hz and 1000 Hz. The best surface roughness of the specimen was achieved at a frequency of 900 Hz with a R_a of 0.287 μm . The aforementioned findings offer a promising foundation for future exploration of vibration-assisted CNC milling. Subsequent investigations should prioritize the execution of an extensive examination

that takes into account the key impacts of machining and vibration elements, as well as their interaction, particularly in relation to cutting situations with specified frequencies utilizing PZT actuators. Through a deep analysis of these variables, the genuine capacity and suitability of vibration-assisted milling may be expansively explored in order to expand production efficacy while dealing with hard materials. Furthermore, the results show that the suggested stage possesses a higher initial natural frequency compared to several preceding stages that applied vibration-assisted milling.

Based on the effectiveness of the proposed stage in a suitable frequency range, further research will investigate fabricated specimens with various hard materials as well as discover the interactions among provided frequencies based on PZT actuators and different cutting conditions so as to find suitable cutting conditions combined with supplied frequencies for enhancing the quality of fabricated surfaces.

This research was limited to investigating the quality response of surface roughness for a vibration-assisted milling process. In future studies, other output quality characteristics of the vibration-assisted milling process will be investigated to evaluate the effectiveness of the proposed positioner.

Author Contributions: Conceptualization, M.P.D.; Methodology, M.P.D. and H.G.L.; Software, M.P.D. and V.Q.A.T.; Validation, M.P.D. and H.G.L.; Formal Analysis, H.V.T.; Investigation, C.T.T. and V.Q.A.T.; Data Curation, M.P.D. and V.Q.A.T.; Writing—Original Draft Preparation, M.P.D.; writing—Review and Editing, M.P.D., H.V.T. All authors have read and agreed to the published version of the manuscript.

Funding: This research was funded by Ho Chi Minh City University of Technology and Education, Vietnam.

Data Availability Statement: The original contributions presented in the study are included in the article, further inquiries can be directed to the corresponding author.

Acknowledgments: The authors acknowledge the support of Ho Chi Minh City University of Technology and Education for this study.

Conflicts of Interest: The authors declare that they have no known competing financial interests or personal relationships that could have appeared to influence the work reported in this paper.

References

1. Lauwers, B.; Klocke, F.; Klink, A.; Tekkaya, A.E.; Neugebauer, R.; Mcintosh, D. Hybrid processes in manufacturing. *CIRP Ann.* **2014**, *63*, 561–583. [[CrossRef](#)]
2. Bulla, B.; Klocke, F.; Dambon, O.; Hünten, M. Ultrasonic assisted diamond turning of hardened steel for mould manufacturing. *Key Eng. Mater.* **2012**, *516*, 437–442. [[CrossRef](#)]
3. Lauwers, B.; Van Gestel, N.; Vanparys, M.; Plakhotnik, D. Machining of ceramics and ecological steels using a mill-turn centre equipped with an ultrasonic assisted tooling system. In Proceedings of the MTTRF 2009 Meeting, Shanghai, China, 8–9 July 2009; pp. 183–200.
4. Heisel, U.; Wallaschek, J.; Eisseler, R.; Potthast, C. Ultrasonic deep hole drilling in electrolytic copper ECu 57. *CIRP Ann.* **2008**, *57*, 53–56. [[CrossRef](#)]
5. Neugebauer, R.; Stoll, A. Ultrasonic application in drilling. *J. Mater. Process. Technol.* **2004**, *149*, 633–639. [[CrossRef](#)]
6. Lian, H.; Guo, Z.; Huang, Z.; Tang, Y.; Song, J. Experimental research of Al6061 on ultrasonic vibration assisted micro-milling. *Procedia Cirp* **2013**, *6*, 561–564. [[CrossRef](#)]
7. Mori, M.; Fujishima, M.; Yohei, O. 5 axis mill turn and hybrid machining for advanced application. *Procedia CIRP* **2012**, *1*, 22–27. [[CrossRef](#)]
8. Xing, D.; Zhang, J.; Shen, X.; Zhao, Y.; Wang, T. Tribological properties of ultrasonic vibration assisted milling aluminium alloy surfaces. *Procedia CIRP* **2013**, *6*, 539–544. [[CrossRef](#)]
9. Zheng, L.; Chen, W.; Huo, D. Experimental investigation on burr formation in vibration-assisted micro-milling of Ti-6Al-4V. *Proc. Inst. Mech. Eng. Part C J. Mech. Eng. Sci.* **2019**, *233*, 4112–4119. [[CrossRef](#)]
10. Phan, N.H.; Muthuramalingam, T.; Trong Ly, N.; Van Dua, T. Effect of ultrasonic low-frequency vibration and its direction on machinability in WEDM process. *Mater. Manuf. Process.* **2022**, *37*, 1045–1051. [[CrossRef](#)]
11. Phan, N.H.; Muthuramalingam, T. Multi criteria decision making of vibration assisted EDM process parameters on machining silicon steel using Taguchi-DEAR methodology. *Silicon* **2021**, *13*, 1879–1885. [[CrossRef](#)]

12. Chen, W.; Huo, D.; Shi, Y.; Hale, J.M. State-of-the-art review on vibration-assisted milling: Principle, system design, and application. *Int. J. Adv. Manuf. Technol.* **2018**, *97*, 2033–2049. [[CrossRef](#)]
13. Brehl, D.E.; Dow, T.A. Review of vibration-assisted machining. *Precis. Eng.* **2008**, *32*, 153–172. [[CrossRef](#)]
14. Dang, M.P.; Le, H.G.; Tran, C.T.; Nguyen, V.D.T.; Chau, N.L. Analysis and Optimization of a Novel Compact Compliant 2-DOF Positioner for Positioning to Assess Bio-Specimen Characteristics. *Machines* **2024**, *12*, 421. [[CrossRef](#)]
15. Ding, B.; Li, X.; Li, C.; Li, Y.; Chen, S. A survey on the mechanical design for piezo-actuated compliant micro-positioning stages. *Rev. Sci. Instrum.* **2023**, *94*. [[CrossRef](#)] [[PubMed](#)]
16. Wu, H.; Tang, H.; Qin, Y. Design and Test of a 2-DOF Compliant Positioning Stage with Antagonistic Piezoelectric Actuation. *Machines* **2024**, *12*, 420. [[CrossRef](#)]
17. Wang, F.; Zhao, X.; Huo, Z.; Shi, B.; Liang, C.; Tian, Y.; Zhang, D. A 2-DOF nano-positioning scanner with novel compound decoupling-guiding mechanism. *Mech. Mach. Theory* **2021**, *155*, 104066. [[CrossRef](#)]
18. Wang, P.; Xu, Q. Design of a flexure-based constant-force XY precision positioning stage. *Mech. Mach. Theory* **2017**, *108*, 1–13. [[CrossRef](#)]
19. Liu, Y.; Zheng, Y.; Gu, Y.; Lin, J.; Lu, M.; Xu, Z.; Fu, B. Development of piezo-actuated two-degree-of-freedom fast tool servo system. *Micromachines* **2019**, *10*, 337. [[CrossRef](#)]
20. Gu, Y.; Duan, X.; Lin, J.; Yi, A.; Kang, M.; Jiang, J.; Zhou, W. Design, analysis, and testing of a novel 2-DOF vibration-assisted polishing device driven by the piezoelectric actuators. *Int. J. Adv. Manuf. Technol.* **2020**, *111*, 471–493. [[CrossRef](#)]
21. Gu, Y.; Chen, X.; Lin, J.; Lu, M.; Lu, F.; Zhang, Z. Vibration-assisted roll-type polishing system based on compliant micro-motion stage. *Micromachines* **2018**, *9*, 499. [[CrossRef](#)]
22. Dang, M.P.; Le, H.G.; Chau, N.L.; Dao, T. An Optimized Design of New XY θ Mobile Positioning Microrobotic Platform for Polishing Robot Application Using Artificial Neural Network and Teaching-Learning Based Optimization. *Complexity* **2022**, *2022*, 2132005. [[CrossRef](#)]
23. Pham, H.T.; Nguyen, V.K.; Dang, Q.K.; Duong, T.V.A.; Nguyen, D.T.; Phan, T.V. Design optimization of compliant mechanisms for vibration assisted machining applications using a hybrid Six Sigma, RSM-FEM, and NSGA-II approach. *J. Mach. Eng.* **2023**, *23*, 135–158. [[CrossRef](#)]
24. Zheng, L.; Chen, W.; Huo, D.; Lyu, X. Design, analysis, and control of a two-dimensional vibration device for vibration-assisted micromilling. *IEEE/ASME Trans. Mechatron.* **2020**, *25*, 1510–1518. [[CrossRef](#)]
25. Kang, D.; Gweon, D. Analysis and design of a cartwheel-type flexure hinge. *Precis. Eng.* **2013**, *37*, 33–43. [[CrossRef](#)]
26. Sun, Y.; Lueth, T.C. Enhancing torsional stiffness of continuum robots using 3-D topology optimized flexure joints. *IEEE/ASME Trans. Mechatron.* **2023**, *28*, 1844–1852. [[CrossRef](#)]
27. Zhang, Q.; Zhao, J.; Shen, X.; Xiao, Q.; Huang, J.; Wang, Y. Design, modeling, and testing of a novel XY piezo-actuated compliant micro-positioning stage. *Micromachines* **2019**, *10*, 581. [[CrossRef](#)] [[PubMed](#)]
28. Dang, M.P.; Le, H.G.; Chau, N.L.; Dao, T. Optimization for a Flexure Hinge Using an Effective Hybrid Approach of Fuzzy Logic and Moth-Flame Optimization Algorithm. *Math. Probl. Eng.* **2021**, *2021*, 6622655. [[CrossRef](#)]
29. Jia, H.; Rao, H.; Wen, C.; Mirjalili, S. Crayfish optimization algorithm. *Artif. Intell. Rev.* **2023**, *56* (Suppl. S2), 1919–1979. [[CrossRef](#)]
30. Sorgente, T.; Biasotti, S.; Manzini, G.; Spagnuolo, M. A survey of indicators for mesh quality assessment. *Comput. Gr. Forum* **2023**, *42*, 461–483. [[CrossRef](#)]
31. Lai, W.; Gao, J.; Zhang, L.; Zhong, Y. Parallel and Decoupled xy Flexible Positioning Platform for Micro Led Panel Repair. In Proceedings of the 2020 21st International Conference on Electronic Packaging Technology (ICEPT), Guangzhou, China, 12–15 August 2020; IEEE: Piscataway, NJ, USA, 2020; pp. 1–6.

Disclaimer/Publisher’s Note: The statements, opinions and data contained in all publications are solely those of the individual author(s) and contributor(s) and not of MDPI and/or the editor(s). MDPI and/or the editor(s) disclaim responsibility for any injury to people or property resulting from any ideas, methods, instructions or products referred to in the content.